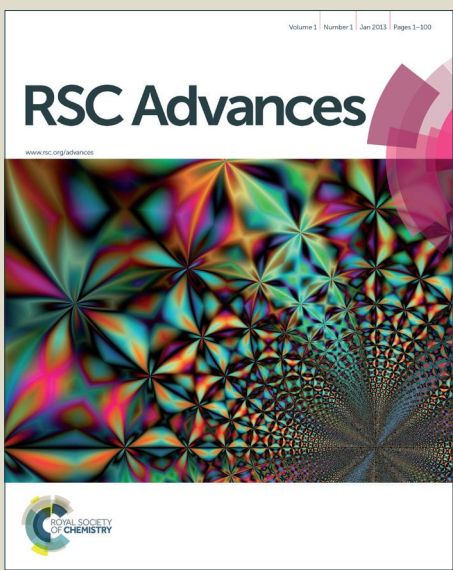
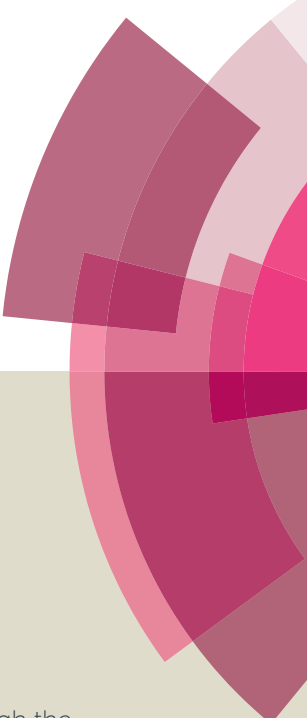


RSC Advances



This is an Accepted Manuscript, which has been through the Royal Society of Chemistry peer review process and has been accepted for publication.

Accepted Manuscripts are published online shortly after acceptance, before technical editing, formatting and proof reading. Using this free service, authors can make their results available to the community, in citable form, before we publish the edited article. This Accepted Manuscript will be replaced by the edited, formatted and paginated article as soon as this is available.

You can find more information about Accepted Manuscripts in the [Information for Authors](#).

Please note that technical editing may introduce minor changes to the text and/or graphics, which may alter content. The journal's standard [Terms & Conditions](#) and the [Ethical guidelines](#) still apply. In no event shall the Royal Society of Chemistry be held responsible for any errors or omissions in this Accepted Manuscript or any consequences arising from the use of any information it contains.



Received 00th January 20xx,
Accepted 00th January 20xx

DOI: 10.1039/x0xx00000x

www.rsc.org

Facile fabrication of N-doped hierarchical porous carbon@CNTs coaxial nanocable with high performance for energy storage and conversion

Yuanyuan Li,^a Wei Xia,^b Ruqiang Zou,^b Jianan Zhang,^{*ac} Zhimin Chen^a and Qun Xu^{*a}

A facile and cost-effective design and fabrication to realize optimal carbon nanoarchitecture containing hierarchical pores appropriate N doping and high conductivity for high-performance in energy storage and conversion is still a challenge. Herein, we have facilely achieved an intriguing heterostructure of N-doped hierarchical porous carbon@CNTs coaxial nanocable (HPNCNTs) via one-step carbonization of resorcinol-melamine-formaldehyde resin (RMF)@CNTs shell@core nanostructures. Significantly, we have demonstrated that the RMF@CNTs shell@core nanostructures with inherent microporous structure and proper N-containing functionalities represents the ideal precursor to realize carbon heterostructure for electrochemical performance optimization on supercapacitors and oxygen reduction reaction (ORR). The results show that the HPNCNTs exhibit the specific capacitance of 284 F g⁻¹, much higher than that of CNTs and most reported N-doped carbons, good rate capability and a robust cycling performance with no capacity fading even after 600 cycles. Furthermore, HPNCNTs shows high electrocatalytic activity ORR with an onset potential of -0.04 V (vs. Ag/AgCl), a dominant four-electron pathway ($n=3.84$), long-term stability, and excellent resistance to crossover effects superior to that of the commercial Pt/C. The present investigation opens the avenue for creating carbon heterostructure with desirable porous tissue and morphology thought a facile and general route for the future high-performance renewable energy storage and conversion devices.

1. Introduction

The design and construction of porous-carbon-based structures have received significant attention concerning their great potential application in energy storage and conversion systems such as supercapacitor and fuel cells, owing to their important features of excellent textural characteristics, high surface area, abundant surface functionalities, and good chemical stability.¹⁻³ However, porous-carbon-based electrodes are suffering from electrode reaction problems related to inner-pore ions-diffusion efficiency. In fact, the accurate mechanism of ion transport process occurring in the porous organization is very complex, because the tortuosity, connectivity, shape of the pores, as well as the nature of the electrolyte and the solid-liquid interface have to be considered.⁴⁻⁶ In this regard, many efforts have been devoted to the synthesis of carbon materials with 3 dimensional (3D) opened hierarchical porous structures that combine multimodal porous tissue, in which the micropores storage the

charges, mesopores offer channels for the rapid mass transport, and macropores act as ion-buffering reservoirs.⁷ To endow hierarchical porous structures and increase surface area several templates or carriers (silica,⁸ zeolite,⁹ SBA-15¹⁰) as well as chemical activation treatment (KOH,¹¹ ZnCl₂ activation¹²) have been commonly required. Despite the expected multimodal porous tissue have been achieved, the complicated synthetic procedure actually hinder the scale up process.¹²⁻¹⁴ Meanwhile, the high distribution of pores would directly block the structure continuity of the carbon materials and thus lead to an opened bandgap, generating an intrinsic barrier that hindered charge transfer. Therefore, the expected superiority for the hierarchical porous carbons over the common carbons for energy storage and conversion is still not obvious.

In order to balance the competition between concentration of porous structure and electronic conductivity, two main strategies have been adopted for improving both the ions-diffusion efficiency and electron-transport kinetics. The first one is the rational combination of continuous graphitic structural carbon nanotubes (CNTs) and porous carbon to configurate nanoarchitecture with enhanced electrical conductivity, higher surface area/volume ratio, and better mechanical stability, thus leading to the high active and stable electrochemical properties.^{15, 16} This has been well demonstrated in the design and synthesis of CNT/porous carbon composites deriving from CNT/polypyrrole,¹⁷ CNT/polyaniline,¹⁸ and CNT/polyacrylonitrile¹⁹ with improv

^a College of Materials Science and Engineering, Zhengzhou University, Zhengzhou 450052 P. R. China. E-mail: zjn@zzu.edu.cn, qunxu@zzu.edu.cn

^b Beijing Key Laboratory of Advanced Battery Materials, Department of Materials Science and Engineering, College of Engineering, Peking University, Beijing 100871, P. R. China.

^c Key Laboratory of Advanced Energy Materials Chemistry (Ministry of Education), Nankai University, Tianjin 300071 P. R. China.

†Electronic Supplementary Information (ESI) available: [details of any supplementary information available should be included here]. See DOI: 10.1039/x0xx00000x

ARTICLE

RSC Advances

performance for supercapacitor, Li ion batteries, and oxygen oxide reaction (ORR).²⁰⁻²² However, the relatively low surface area of the reported CNT/carbon composites, caused by the poor CNT dispersion in solution and weak interaction of decorated carbon precursor with the CNT surface, greatly suppress electrode reaction kinetics.²³ As an attractive alternative, heteroatom doped carbons, e.g. nitrogen (N) doped carbon, are highlighted by their improved conductivity and high active reactivity for pseudocapacitance and ORR due to that the electron states of N containing species within the carbon lattice can break the electroneutrality of carbon.²⁴ But to well understand the effect of the N species types and contents on enhancing energy storage and conversion is still a great challenge because of the difficulties in controlling the N-doping by the existing method. Undoubtedly, it will be of great significance to simply construct well-defined 1D CNTs/porous carbon architecture with hierarchical pores, high surface area, and optimal N species doping, which can afford both efficient mass and charges exchange, high reaction activity, and conductivity to boost electrochemical and catalytic performance.

Herein, we demonstrated a facile, cost-effective approach to synthesize hierarchical porous N-doped carbon@CNTs coaxial nanocables (HPNCNTs) by direct carbonization of the well-defined microporous resorcinol-melamine-formaldehyde (RMF) coated CNTs nanostrucutres, without any additional templates and activation processes. Significantly, the obtained HPNCNTs simultaneously offer ordered high conductivity of CNTs and 3D hierarchical porous texture combines macropores reservoir, mesoporous and microporous walls. Furthermore, by adjusting the added amount of melamine and annealing temperatures, the N species doping can be appropriated controlled. In these design, three electrochemical processes are involved, that is, transporting electrons along the CNTs cores, diffusing electrolyte ions within the multilevel porous sheaths, and electrochemical reaction on the optimal N species center. As a result, the HPNCNTs exhibit the specific capacitance of 284 F g⁻¹, much higher than that of CNTs and most reported N-doped carbons, good rate capability and a robust cycling performance (99.0% capacitance retention even after 6000 cycles at a high current density of 2 A g⁻¹). Furthermore, HPNCNTs shows high electrocatalytic activity ORR with an onset potential of -0.04 V (vs. Ag/AgCl), a dominant four-electron pathway ($n=3.84$), long-term stability, and excellent resistance to crossover effects superior to that of the commercial Pt/C. This work highlighted the facile and general synthetic strategy for synthesizing core-shell structured carbon with rational porous tissue and morphology for enhancing energy storage and conversion devices.

2. Experimental section

2.1 Synthesis of HPNCNTs

Single-wall CNTs were first pre-treated in a HNO₃/H₂SO₄ (v/v=1:3) mixed solution and refluxing at 70 °C for 2 h. The obtained solid was filtered using filter polytetrafluoroethylene membrane, and washed with deionized water until the pH of the

filtrate reached 7 followed by drying in vacuum at 60 °C for 4 h. For the preparation of HPNCNTs, 0.37 mL of formaldehyde (37 wt %) and 0.275 g of resorcinol were added a mixture containing 30 mg CNTs, 50 mL of water, 20 mL of ethanol and 0.25 mL of ammonia at 70 °C under stirring. After 30 min, 0.13 g melamine and 1.105 mL of formaldehyde were added to the above mixture and continued stirring for another 24 h, followed by hydrothermal treatment at 120 °C for 24 h. The obtained resorcinol-melamine-formaldehyde coated CNTs (RMF@CNTs) were collected by centrifugation, washed with ethanol and water for several times, and dried 60 °C. To obtain HPNCNTs, RMF@CNTs precursors were pyrolyzed at 800 °C for 2 h with a heating rate of 5 °C min⁻¹ under N₂ atmosphere. We also prepared a series of samples at the pyrolysis temperatures of 600 °C, 700 °C and 900 °C, and they were named S-600, S-700 and S-900, respectively.

For comparison, N-doped carbon (NCs) was also prepared using the similar protocol of HPNCNTs without the CNTs. In order to show the superiority of RMF as carbon precursor for electrochemical applications, several kinds of nitrogen-doped carbon@CNTs nanostructures were prepared using polypyrrole and polyaniline as carbon precursors,^{18,25} which are denoted as NC-CNTs-PPy and NC-CNTs-PANI, respectively.

2.2 Characterizations

The morphology of the samples was studied by a field-emission scanning electron microscope (FE-SEM, JEOL JSM-6700F) and a transmission electron microscope (TEM, FEI Tecnai G2 20) with an accelerating voltage of 200 kV. Powder X-ray diffraction (XRD) patterns were collected using a Y-2000X-ray Diffractometer using copper K α radiation ($\lambda=1.5406 \text{ \AA}$) at 40 kV, 40 mA. The X-ray photoelectron spectroscopy (XPS) measurements were performed with an ESCA LAB 250 spectrometer using a focused monochromatic Al K α line (1486.6 eV) X-ray beam with a diameter of 200 μm . The Raman measurements were performed on a Renishaw spectrometer at 532 nm on a Reishaw Microscope System RM2000. The nitrogen sorption measurements at 77 K were carried out by using a Micromeritics Tristar 2020 system with micropore analysis. Before the sorption tests, samples were degassed at 250 °C for 8 h under dynamic vacuum. The Brunauer-Emmett-Teller (BET) specific surface area was calculated using adsorption data at a relative pressure range of P/P₀ = 0.05-0.25. The pore volumes were estimated from the amounts adsorbed at a relative pressure (P/P₀) of 0.99. Pore size distributions were fitted from Quenched Solid Density Functional Theory (QSDFT) based on the desorption branches.

2.3 Electrochemical characterization

2.3.1 Capacitance measurements

The test electrodes were prepared by loading a slurry consisting of 80 wt % active materials, 10 wt % carbon black, and 10 wt % poly (tetrafluoroethylene) (used as a binder, PTFE 60 wt % dispersion in H₂O, Sigma-Aldrich) on a nickel foam (1×1 cm²) and dried at 80 °C for 24 h. As-made electrodes were pressed at a pressure of 10 M Pa for 1 min. The electrochemical properties of samples were measured in a three-electrode cell in 6.0 M KOH aqueous solution with the smaller electrode as the test

electrode, platinum foil as the counter electrode, Ag/AgCl electrode as the reference electrode. The cyclic voltammetry (CV) curves were obtained at various scan rates with voltage ranging from -1 V to 0 V. The chronopotentiometry (CP) curves were obtained at various current densities with the same voltage range as CV. The electrochemical impedance spectroscopy (EIS) was measured in the frequency range of 10 m Hz to 10 kHz at the open circuit voltage with an alternate current amplitude of 5 mV. All measurements were carried out on a CHI 660D electrochemical workstation (CHI Instruments Inc.) at room temperature.

2.3.2 Electrocatalysis characterization

For the preparation of working electrodes, 1 mg of catalyst was dispersed in 1 mL of ethanol under sonication for 1 h to form a homogeneous catalyst ink. Then 20 μ L of this catalyst ink was loaded onto a glassy carbon rotating disk electrode (diameter is 5 mm), resulting in the catalyst loading of 0.1 mg cm⁻², followed by drying at room temperature. After air-drying, the electrode was added dropwise 5 μ L of 0.1 wt% Nafion on suspension in ethanol as a binder.

ORR measurements were conducted using cyclic voltammetry and linear sweep voltammetry measurements by a CHI electrochemical workstation (Model 760C) with a standard three-electrode system. The catalyst-coated glassy carbon electrode was used as the working electrode, and an Ag/AgCl electrode in saturated KCl solution and Pt wire work as the reference and counter electrodes, respectively. The electrolyte was 0.1 M potassium hydroxide (KOH) aqueous solution. All electrochemical measurements were performed at room temperature.

Koutecky-Levich plots were analyzed at different potentials. The electron transfer numbers during the oxygen reduction reaction (ORR) were calculated from the slopes of their linear-fit lines based on the Koutecky-Levich equation:

$$\frac{1}{J} = \frac{1}{J_L} + \frac{1}{J_K} = \frac{1}{B\omega^{0.5}} + \frac{1}{J_K} \quad (1)$$

$$B = 0.62nFC_0(D_0)^{2/3}\nu^{-1/6} \quad (2)$$

$$J_K = nFkC_0 \quad (3)$$

Where J is the measured current density, J_L and J_K are the diffusion- and kinetic-limiting current densities, ω is the rotation speed (rad s^{-1}), n is the transferred electron number, F is the Faraday constant ($96\ 485\ \text{C mol}^{-1}$), C_0 is the O_2 concentration in the electrolyte ($1.26 \times 10^{-6}\ \text{mol cm}^{-3}$), D_0 is the diffusion coefficient of O_2 in the electrolyte ($1.93 \times 10^{-5}\ \text{cm}^2\ \text{s}^{-1}$), and μ is the kinetic viscosity of 0.1 M perchloric acid ($0.01009\ \text{cm}^2\ \text{s}^{-1}$).

3. Results and discussion

Recent studies reveal that resorcinol-melamine-formaldehyde resins nanostructure have attracted tremendous attentions because of its intrinsic microporous structures and controllable structures, which are widely used for gas (CO_2 , H_2) adsorptions.²⁶ Such interesting feature will be advantageous

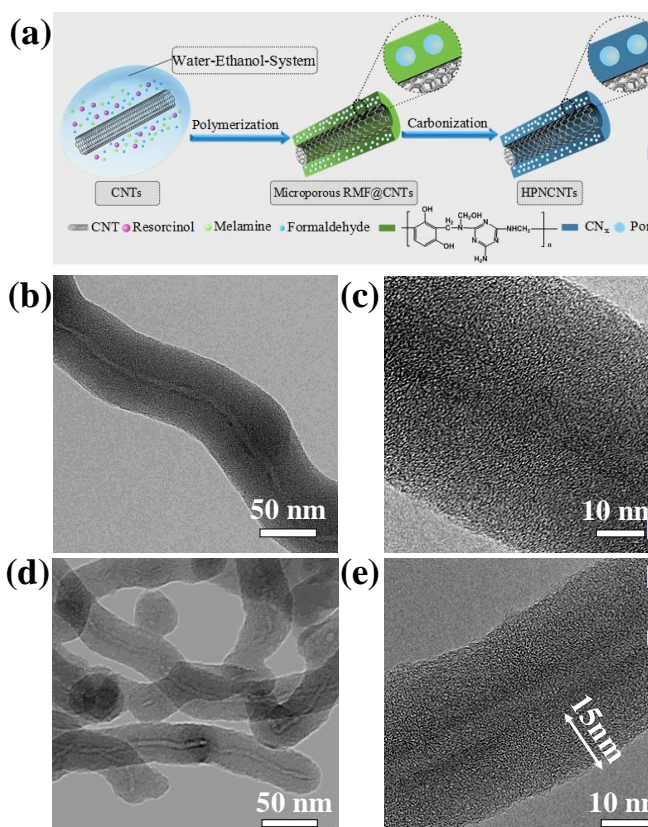


Fig. 1(a) Schematic illustration of the synthesis of HPNCNTs. **TEM images of (b-c)** microporous RMF@CNTs, **(d-e)** HPNCNTs-800.

for achieving high porosity and surface area in carbon nanostructures. Here, we facilely prepare hierarchical porous N-doped HPNCNTs using microporous resorcinol-melamine-formaldehyde (RMF) coated CNTs nanostructures as precursor, as illustrated in **Fig. 1a**. The formation process of RMF@CNTs is based on an extended Stöber method.²⁶⁻²⁸ In the first stage, a condensation occurs among the hydroxy methyl groups between MF and RF precursors, ammonia, and alcohol to form methylene and methylene ether bridged polymeric clusters,²⁶ which can combine with CNTs via the surface-COOH and -OH groups. The second stage in the formation of a continuous RMF sheath on the surface of CNTs is initiated by the polymerization of MF and RF precursors around the small clusters under hydrothermal conditions. **Fig. S1a** shows the pristine CNTs with a diameter of about 10 nm. Then, the RMF@CNTs coaxial nanocables formed by an in-situ polymerization and assembly process of resorcinol, melamine, and formaldehyde on the surface of CNTs under an extent Stöber condition. As shown in **Fig. 1b&c**, a compact core-shell structure of RMF@CNTs have the RMF sheath with a thickness of ~25 nm. Particularly, the larger magnified TEM image (**Fig. 1c**) obviously reveals the microporous structure of the RMF resin sheath. After carbonization at 600-900 °C, all samples can keep a 1D core-shell nanocable morphology and porous structure (**Fig. 1d&e**, **S1b-e**). For example, the HPNCNTs carbonized at 800 °C with a shrinking carbon sheath of ~15 nm (**Fig. 1e**). As a comparison, the pure N-doped carbons

ARTICLE

RSC Advances

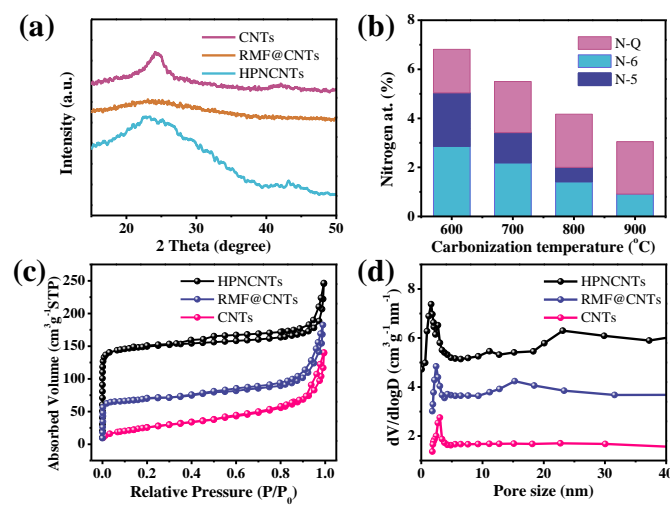


Fig. 2 (a) XRD patterns of CNTs, microporous RMF@CNTs and HPNCNTs. (b) The atomic concentration of different N-functional groups with different treatment temperature. (c) N_2 adsorption and desorption isotherms and (d) pore size distribution.

(NCs) was also obtained via the above synthetic strategy without the CNTs, which are conjugated microspheres as seen in the SEM image (**Fig. S1f**).

The structural characterizations of HPNCNTs are further monitored by XRD, Raman, XPS, BET measurements. The XRD pattern of the HPNCNTs (**Fig. 2a**) exhibits two obvious peaks at 25° and 43° , assigned to the (002) and (100) planes of the hexagonal carbon material,²⁹ respectively, suggesting that the RMF layer on the CNTs has been carbonized. The Raman spectrum of the HPNCNTs (**Fig. S2**) displays a higher ratio of I_D/I_G (I_D and I_G are related to the A_{1g} vibration mode of the disordered carbon (D-bond) and the E_{2g} vibration mode of the ordered graphitic carbon (G-bond)) compared to that of CNTs because of the incorporated N atoms.³⁰ **Fig. S3&S4** depict XPS survey spectrum and N1s spectrum for HPNCNTs. Compared with CNTs, a pronounced N1s peak (ca. 400 eV) is clearly observed. The contents of each element are summarized in **Table S1**. The spectra can be deconvoluted into three peaks, which correspond to pyridinic N (398.9 eV), pyrrolic N (400.4 eV), graphitic N (401.3 eV), respectively.³¹ As shown in **Fig. 2b**, for S-600, pyrrolic N and pyridinic N species are predominant together with a few graphitic N species. As the temperature increases, the unstable pyrrolic N atom gradually transforms a graphitic N atom.³¹ However, graphitic N species are yet relatively low in S-700. Particularly, the HPNCNTs possess mainly graphitic N, pyridinic N, and less pyrrolic N species. The greater amount of graphitic N can promote the four-electron process in the ORR and enhance the conductivity in electrode materials of supercapacitors. Meanwhile, these accessible species of pyridinic N and pyrrolic N would provide chemically active sites for the pseudocapacitive reaction. For S-900, although it has a high content of graphitic N, the overall N content is fairly low, the pyridinic N is significantly reduced and the pyrrolic N is vanished. On the basis of the XPS data, the HPNCNTs are expected to have a higher performance than others for ORR and supercapacitors.

N_2 adsorption-desorption analyses give more quantitative set of information on the porous structures of the samples (**Fig. 2c**). The CNTs have a type III adsorption isotherm with an H3 hysteresis loop at $P/P_0 = 0.9\text{--}1.0$, indicating that the slit-shaped mesopores raised from the packing of CNT aggregates. In contrast, HPNCNTs and RMF@CNTs show the type I with a well-defined knee at low P/P_0 (0.0–0.1), implying the existence of a microspore. While the isotherm changes to type IV at $P/P_0 = 0.45\text{--}1$, indicating the presence of a certain portion of mesopores and macropores.³² As listed in **Table S2**, we surprisingly find that wrapped with RMF sheath, the BET surface area of CNTs ($99.4 \text{ m}^2 \text{ g}^{-1}$) greatly increased to $228.6 \text{ m}^2 \text{ g}^{-1}$, and HPNCNTs are measured to be $663 \text{ m}^2 \text{ g}^{-1}$, which are higher than those of previously reported 1D hybrid carbon materials without any active treatment (**Table S3**). It is noticed that the BET data further demonstrates our rational design of using microporous RMF@CNTs as carbon precursor to pursue carbon materials with high surface area. The pore size distribution (PSD) for adsorption data is given in **Fig. 2d** and **Table S2**. The pristine CNTs show a pore size of 2.4 nm, which might be attributed to the end pores of the CNTs. The RMF@CNTs contains relatively high micropores and less mesopores, which is consistent with the above results of TEM observation (**Fig. 1c**). It can be seen that the HPNCNTs have not only sharp peaks at 1.9 and 2.8 nm, but also slightly sharp peaks at 13.0, 22.0 and 51.7 nm, indicating the coexistence of hierarchical micropores, mesopores and macropores in the HPNCNTs. The macroporous structure of HPNCNTs is probably derived from the interconnected network of the nanocables. Such a multi-model porous structure will be significant for the rapid mass diffusion of charges and electrolyte, thus leading to a high capacitance and electrocatalytic activity.

The unique structure of the HPNCNTs inspired us to evaluate their electrochemical performance for supercapacitors with a three-electrode system in a 6 M KOH aqueous

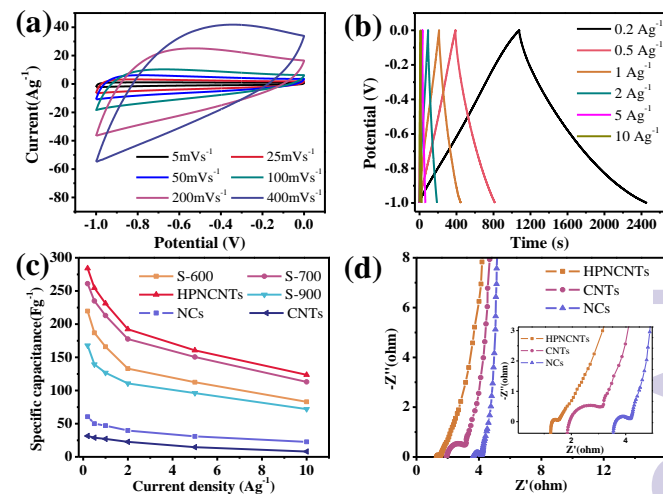


Fig. 3 Electrochemical performances measured in a three-electrode system. (a) CV of the HPNCNTs electrode at different scan rates. (b) Galvanostatic charge-discharge curves of HPNCNTs at different current densities. (c) Specific capacitances of different electrodes at different current densities. (d) Electrochemical impedance spectra measured in the frequency range of 10 mHz to 10 kHz.

electrolyte (**Fig. 3**). As seen in **Fig. 3a**, HPNCNTs present roughly rectangular-like shapes and reversible bumps in CV curves, suggesting the combination of electric double-layer capacitance (EDLC) and pseudocapacitive reaction.^{33, 34} It should be noticed that the rectangular shape of HPNCNTs maintains even at a high potential scan rate of 400 mV s⁻¹, indicating the pure EDLC behaviour and the rapid formation of the double-layer even at high rates.

Furthermore, the galvanostatic charge-discharge curves (**Fig. 3b**) show the approximately triangular symmetrical distribution with a gradual slope change, exhibiting an ideal capacitor behavior. Combining the hierarchical porous structure, optimized N-doping, and high conductivity, HPNCNTs exhibit the highest specific capacitance of is 284 F g⁻¹ at 0.2 A g⁻¹ than other samples, and even 7.6 and 4.7 times higher than that of the CNTs (37 F g⁻¹) and NCs (60.4 F g⁻¹) (**Fig. 3c**). The enhanced conductivity of HPNCNTs can further demonstrated by the Nyquist plots (**Fig. 3d**). Typically, HPNCNTs exhibit a lower resistance (1.3 Ω) than the CNTs (1.9 Ω) and NCs (3.5 Ω), suggesting a higher conductivity of the HPNCNTs. It is generally accepted that the IR drop is related to the electrical conductivity and porous texture (including the connectivity, size distribution, shape of pores) of the electrode. Therefore, the lower IR drop of HPNCNTs than that of CNTs and NCs can be attributed to the synergy of rapid mass transport pathway of hierarchical porous structured sheath and high conductive CNT core. In the case of NCs, and CNTs, the lack of ordered electron migration channel (for NCs) or very short inner-pore transport pathway (for CNTs) will inevitably lead to a significant ionic diffusion loss contribution to the high resistance. As a result, HPNCNTs shows the highest specific capacitance. **Fig. 4a&b** present the cycling performance of HPNCNTs at current density of 2 A g⁻¹. HPNCNTs exhibits a very stable capacitance (99.0% of the original capacitance) after 6000 cycles of charging and discharging, indeed indicating its long-term electrochemical stability. This is further conformed by the inconspicuous change between charging-discharging curves of first and 6000th cycle. According to **Table S4**, the HPNCNTs have the best supercapacitor performance in most reported the state-of-the-art carbon materials electrodes.

To verify the optimization of N-doped and porous tissue of HPNCNTs, N-doped porous carbon@CNTs coaxial materials derived from polyaniline and polypyrrole are also prepared, which are named as NC-CNTs-PANI and NC-CNTs-PPy,

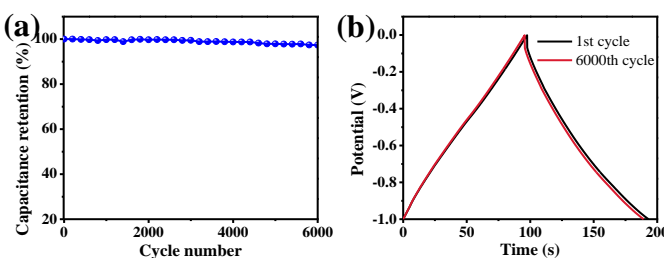


Fig. 4 (a) Capacitance retention vs. cycle number of HPNCNTs measured at 2 A g⁻¹. (b) Galvanostatic charge/discharge curves of HPNCNTs before and after 6000 cycles measured at 2 A g⁻¹.

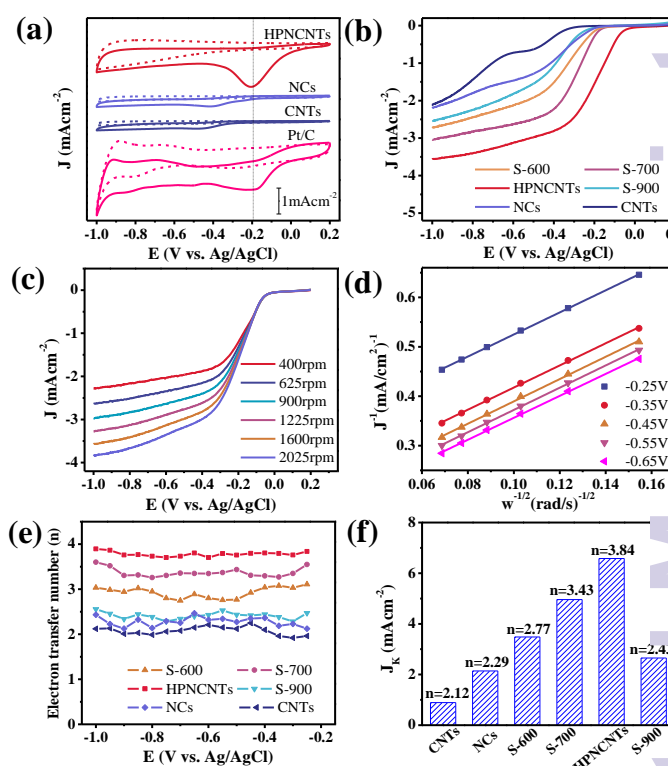


Fig. 5 Electrocatalytic activity in ORR in 0.1 M KOH. The loading was 0.1 mg cm⁻² for all materials. (a) CV curves in N₂-saturated (dashed curves) and O₂-saturated (solid curves) solution (b) RDE polarization curves at a rotation rate of 1600 rpm. (c) RDE polarization curves for HPNCNTs at different rotation speeds. (d) The K-L plots derived from HPNCNTs. (e) The electron transfer number as a function of potential. (f) Electrocatalytic activity given as the kinetic current density (J_k) at 0.5 V for all samples.

respectively. Obviously, the HPNCNTs present high capacitive behavior with longer charge-discharge time (**Fig. S5a**). Particularly, the HPNCNTs display a substantially higher specific capacitance than NC-CNTs-PANI (86 F g⁻¹) and NC-CNTs-PPy (58 F g⁻¹) (**Fig. S5b**). As demonstrated by the above results, the superb capacitance of HPNCNTs could be due to the synergistic effects of an optimal N-doping, a large accessible surface area and the high conductivity of RMF@CNTs derived carbon nanostructures. Taking into account of their high specific capacitance and the very robust electrochemical stability, the HPNCNTs present promise as the advanced electrode candidate for supercapacitor.

The HPNCNTs can also work well for ORR. Cyclic voltammetry (CV) measurements of HPNCNTs, S-600, S-700, S-900, NCs and CNTs in N₂-saturated and O₂-saturated were performed in 0.1 M KOH (**Fig. 5a & S6**). Compared with their featureless character in N₂-saturated solution, catalytic peaks are found in O₂-saturated solutions. Moreover, a well-defined oxygen reduction cathodic peak at about -0.2 V can be clearly observed for HPNCNTs in O₂-saturated solution, while the corresponding reduction peak for S-600, S-700, S-900, NCs and CNTs shifts negatively to -0.3 V, -0.42 V, -0.62 V, -0.49 V and -0.55 V, respectively. This value is positively shifted about 100 mV, 220 mV, 420 mV, 290 mV and 350 mV compared to S-600, S-700, S-900, NCs and CNTs, indicating an effective

ARTICLE

RSC Advances

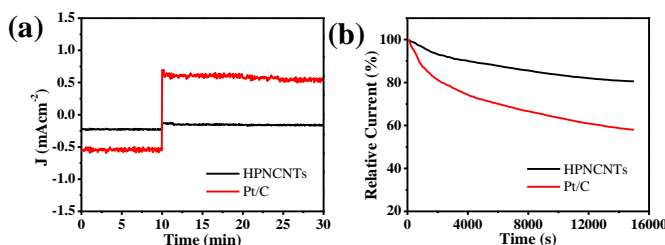


Fig. 6 (a) Methanol crossover effect test upon addition of 3 M methanol at -0.3 V.
(b) Stability evaluation at -0.3 V and a rotation speed of 1600 rpm.

electrochemical reduction of oxygen for HPNCNTs. To further investigate the ORR catalytic activity, rotating disk electrode (RDE) tests were performed. The ORR onset potentials of each sample were acquired from the RDE linear sweep (**Fig. 5b**). The highest onset potential and largest cathodic current density are harvested by HPNCNTs. Although these are slightly lower than that of Pt/C electrode, just as the case for other N-containing carbon materials for the ORR,^{35, 36} the onset potential of the ORR on the HPNCNTs (-0.04 V) also has positive shift compared with the NCs and CNTs, and most previous reports on N-doped carbon materials.^{37, 38}

RDE experiments at different rotating speeds were also carried out (**Fig. 5c** and **Fig. S7**) and the kinetic parameters are analyzed with the Koutecky-Levich (K-L) equation. The limit current density of HPNCNTs for ORR was gradually increased with higher rotation speed. Furthermore, the corresponding K-L plots display good linearity and near parallelism at various potentials (**Fig. 5d**), which implied first-order reaction kinetics to the dissolved oxygen concentration. In the ORR, oxygen can be reduced via two reaction pathways, four- and two-electron transfer processes, in which the four-electron transfer process is preferred. As seen in **Fig. 5e**, the HPNCNTs show the highest and nearly stable electron transfer number with an average value of 3.85 in the potential range from -1 to -0.25 V, which is close to that of commercial Pt/C catalyst (20% Pt supported on Vulcan XC-72 carbon, Johnson Matthey) of 4. As shown in **Fig. 5f**, the calculated J_K value (6.58 mA cm⁻²) of HPNCNTs at -0.50 V is much higher than that of S-600 (3.48 mA cm⁻²), S-700 (4.96 mA cm⁻²), S-900 (2.65 mA cm⁻²), NCs (2.14 mA cm⁻²), and CNTs (0.89 mA cm⁻²), and is even higher than previous reports on N-doped carbon materials.³⁹

The resistance to methanol crossover effects and durability is a key factor for their practical application in fuel cells.⁴⁰ Thus, the chronoamperometric responses of HPNCNTs and Pt/C upon addition of 3 M methanol are carried out (**Fig. 6a**). With the adding of methanol, the better stability of HPNCNTs for ORR can be demonstrated from their negligible current decay, indicating the superior tolerance against methanol crossover over commercial Pt/C catalyst. Furthermore, the cycle stability of HPNCNTs and Pt/C catalyst is tested at -0.3 V for 15000 s (**Fig. 6b**). HPNCNTs exhibited a very low attenuation of 18% current loss while that for Pt/C is 42%, indicating a superior stability of HPNCNTs. Therefore, HPNCNTs shows a promising candidate for ORR due to its high catalytic activity, stability, and selectivity.

4. Conclusions

In summary, hierarchical porous N-doped carbon@CNTs coaxial nanocables were successfully synthesized by a facile approach of direct carbonization of microporous resorcinol-melamine-formaldehyde (RMF)@CNTs shell@core nanostructure. Significantly, the obtained HPNCNTs combine the unique features of 1D core@shell nanostructure, multimodal porosity, high specific surface area, and optimal N composition and content, giving robust electrochemical performance for supercapacitor as well as excellent electrocatalytic activity towards the ORR. The present work opens the door for engineering in hierarchical porous N-doped carbon nanoarchitectures through a facile and general route without any additional templates and activation processes for high-performance renewable energy storage and conversion.

Acknowledgements

This work was financially supported by the National Natural Science Foundation of China (Nos. 21571157, 51173170, and 51473149), Program for New Century Excellent Talents in Universities (NCET), the Open Project Foundation of Key Laboratory of Advanced Energy Materials Chemistry of Nankai University (2015-32).

Notes and references

- 1 G. Wu, D. Li, C. Dai, D. Wang and N. Li, *Langmuir*, 2008, **24**, 3566-3575.
- 2 Z. Wen, J. Liu and J. Li, *Adv. Mater.*, 2008, **20**, 743-747.
- 3 J.-S. Yu, S. Kang, S. B. Yoon and G. Chai, *J. Am. Chem. Soc.*, 2002, **124**, 9382-9383.
- 4 G.-J. Lee and S.-I. Pyun, *Langmuir*, 2006, **22**, 10659-10665.
- 5 J. W. Long, B. Dunn, D. R. Rolison and H. S. White, *Chem. Rev.*, 2004, **104**, 4463-4492.
- 6 D. R. Rolison, *Science*, 2003, **299**, 1698-1701.
- 7 S. Wang, J. Zhang, P. Shang, Y. Li, Z. Chen and Q. Xu, *Chem. Commun.*, 2014, **50**, 12091-12094.
- 8 K. Kwon, Y. J. Sa, J. Y. Cheon and S. H. Joo, *Langmuir*, 2012, **28**, 991-996.
- 9 C. O. Ania, V. Khomenko, E. Raymundo-Piñero, J. B. Parra and F. Béguin, *Adv. Funct. Mater.*, 2007, **17**, 1828-1836.
- 10 W. Kim, M. Y. Kang, J. B. Joo, N. D. Kim, I. K. Song, P. Kim, J. R. Yoon and J. Yi, *J. Power Sources*, 2010, **195**, 2125-2129.
- 11 F. Su, C. K. Poh, J. S. Chen, G. Xu, D. Wang, Q. Li, J. Lin and X. W. Lou, *Energy Environ. Sci.*, 2011, **4**, 717-724.
- 12 C. Vix-Guterl, E. Frackowiak, K. Jurewicz, M. Friebel, J. Parmentier and F. Béguin, *Carbon*, 2005, **43**, 1293-1302.
- 13 H. Zhu, J. Yin, X. Wang, H. Wang and X. Yang, *Adv. Funct. Mater.*, 2013, **23**, 1305-1312.
- 14 S. Pylypenko, T. S. Olson, N. J. Carroll, D. N. Petsev and P. Atanassov, *J. Phys. Chem. C*, 2010, **114**, 4200-4207.
- 15 C.-M. Chuang, C.-W. Huang, H. Teng and J.-M. Ting, *Energy & Fuels*, 2010, **24**, 6476-6482.
- 16 M. Noked, S. Okashy, T. Zimrin and D. Aurbach, *Angew. Chem., Int. Ed.*, 2012, **51**, 1568-1571.
- 17 K. Shi, M. Ren and I. Zhitomirsky, *ACS Sustainable Chem. Eng.*, 2014, **2**, 1289-1298.
- 18 L. Li, G. Li and B. An, *RSC Adv.*, 2014, **4**, 9756-9761.
- 19 H. Peng, G. Ma, K. Sun, J. Mu, Z. Zhang and Z. Lei, *J. Phys. Chem. C*, 2014, **118**, 29507-29516.

- 20 A. Izadi-Najafabadi, T. Yamada, D. N. Futaba, M. Yudasaka, H. Takagi, H. Hatori, S. Iijima and K. Hata, *ACS Nano*, 2011, **5**, 811-819.
- 21 Y. Yao, C. Ma, J. Wang, W. Qiao, L. Ling and D. Long, *ACS Appl. Mater. Interfaces*, 2015, **7**, 4817-4825.
- 22 Q. Liu, Z. Pu, C. Tang, A. M. Asiri, A. H. Qusti, A. O. Al-Youbi and X. Sun, *Electrochem. Commun.*, 2013, **36**, 57-61.
- 23 G. Xu, B. Ding, P. Nie, L. Shen, J. Wang and X. Zhang, *Chem.-Eur. J.*, 2013, **19**, 12306-12312.
- 24 P. Yu, Y. Li, X. Zhao, L. Wu and Q. Zhang, *Langmuir*, 2014, **30**, 5306-5313.
- 25 B. An, S. Xu, L. Li, J. Tao, F. Huang and X. Geng, *J. Mater. Chem. A*, 2013, **1**, 7222-7228.
- 26 H. Zhou, S. Xu, H. Su, M. Wang, W. Qiao, L. Ling and D. Long, *Chem. Commun.*, 2013, **49**, 3763-3765.
- 27 J. Liu, S. Z. Qiao, H. Liu, J. Chen, A. Orpe, D. Zhao and G. Q. Lu, *Angew. Chem., Int. Ed.*, 2011, **50**, 5947-5951.
- 28 H. T. Chung and P. Zelenay, *Chem. Commun.*, 2015, **51**, 13546-13549.
- 29 C. X. Guo, H. B. Yang, Z. M. Sheng, Z. S. Lu, Q. L. Song and C. M. Li, *Angew. Chem., Int. Ed.*, 2010, **49**, 3014-3017.
- 30 Y. Guo, S. Guo, J. Ren, Y. Zhai, S. Dong and E. Wang, *ACS Nano*, 2010, **4**, 4001-4010.
- 31 J. Pels, F. Kapteijn, J. Moulijn, Q. Zhu and K. Thomas, *Carbon*, 1995, **33**, 1641-1653.
- 32 F. Zhang, Y. Meng, D. Gu, Y. Yan, Z. Chen, B. Tu and D. Zhao, *Chem. Mater.*, 2006, **18**, 5279-5288.
- 33 M. Seredych, D. Hulicova-Jurcakova, G. Q. Lu and T. J. Bandosz, *Carbon*, 2008, **46**, 1475-1488.
- 34 D. Hulicova - Jurcakova, M. Seredych, G. Q. Lu and T. J. Bandosz, *Adv. Funct. Mater.*, 2009, **19**, 438-447.
- 35 Z. Lin, G. Waller, Y. Liu, M. Liu and C. P. Wong, *Adv. Energy Mater.*, 2012, **2**, 884-888.
- 36 S. Wang, E. Iyyamperumal, A. Roy, Y. Xue, D. Yu and L. Dai, *Angew. Chem., Int. Ed.*, 2011, **50**, 11756-11760.
- 37 C. Xiong, Z. Wei, B. Hu, S. Chen, L. Li, L. Guo, W. Ding, X. Liu, W. Ji and X. Wang, *J. Power Sources*, 2012, **215**, 216-220.
- 38 P. Chen, T. Y. Xiao, Y. H. Qian, S. S. Li and S. H. Yu, *Adv. Mater.*, 2013, **25**, 3192-3196.
- 39 L. Qu, Y. Liu, J.-B. Baek and L. Dai, *ACS Nano*, 2010, **4**, 1321-1326.
- 40 R. Liu, D. Wu, X. Feng and K. Müllen, *Angew. Chem., Int. Ed.*, 2010, **122**, 2619-2623.